

A 4H-SiC merged P-I-N Schottky with floating back-to-back diode

Wei-Zhong Chen(陈伟中), Hai-Feng Qin(秦海峰), Feng Xu(许峰), Li-Xiang Wang(王礼祥), Yi Huang(黄义), and Zheng-Sheng Han(韩郑生)

Citation: Chin. Phys. B, 2022, 31 (**2**): 028503. DOI: 10.1088/1674-1056/ac0e23

Journal homepage: http://cpb.iphy.ac.cn; http://iopscience.iop.org/cpb

What follows is a list of articles you may be interested in

Improved 4H-SiC UMOSFET with super-junction shield region

Pei Shen(沈培), Ying Wang(王颖), Xing-Ji Li(李兴冀), Jian-Qun Yang(杨剑群), Cheng-Hao Yu(于成浩), and Fei Cao(曹菲)

Chin. Phys. B, 2021, 30 (**5**): 058502. DOI: 10.1088/1674-1056/abd740

Characteristics and mechanisms of subthreshold voltage hysteresis in 4H-SiC MOSFETs

Xi-Ming Chen(陈喜明), Bang-Bing Shi(石帮兵), Xuan Li(李轩), Huai-Yun Fan(范怀云), Chen-Zhan Li(李诚瞻), Xiao-Chuan Deng(邓小川), Hai-Hui Luo(罗海辉), Yu-Dong Wu(吴煜东), and Bo Zhang(张波)

Chin. Phys. B, 2021, 30 (**4**): 048504. DOI: 10.1088/1674-1056/abd391

Lateral depletion-mode 4H-SiC n-channel junction field-effect transistors operational at 400 ˚C

Si-Cheng Liu(刘思成), Xiao-Yan Tang(汤晓燕), Qing-Wen Song(宋庆文), Hao Yuan(袁昊), Yi-Meng Zhang(张艺蒙), Yi-Men Zhang(张义门), and Yu-Ming Zhang(张玉明)

Chin. Phys. B, 2021, 30 (**2**): 028503. DOI: 10.1088/1674-1056/abc0df

Performance improvement of 4H-SiC PIN ultraviolet avalanche photodiodes with different intrinsic layer thicknesses

Xiaolong Cai(蔡小龙), Dong Zhou(周东), Liang Cheng(程亮), Fangfang Ren(任芳芳), Hong Zhong(钟宏), Rong Zhang(张荣), Youdou Zheng(郑有炓), Hai Lu(陆海)

Chin. Phys. B, 2019, 28 (**9**): 098503. DOI: 10.1088/1674-1056/ab343f

Design and fabrication of 10-kV silicon-carbide p-channel IGBTs with hexagonal cells and step space modulated junction termination extension

Zheng-Xin Wen(温正欣), Feng Zhang(张峰), Zhan-Wei Shen(申占伟), Jun Chen(陈俊), Ya-Wei He(何亚伟), Guo-Guo Yan(闫果果), Xing-Fang Liu(刘兴昉), Wan-Shun Zhao(赵万顺), Lei Wang(王雷), Guo-Sheng Sun(孙国胜), Yi-Ping Zeng(曾一平)

Chin. Phys. B, 2019, 28 (**6**): 068504. DOI: 10.1088/1674-1056/28/6/068504

A 4H-SiC merged P–I–N Schottky with floating back-to-back diode

Wei-Zhong Chen(陈伟中)[1,2], Hai-Feng Qin(秦海峰)[1,†], Feng Xu(许峰)[1],
Li-Xiang Wang(王礼祥)[1], Yi Huang(黄义)[1], and Zheng-Sheng Han(韩郑生)[2,3]

[1] *College of Electronics Engineering, Chongqing University of Posts and Telecommunications, Chongqing* 400065, *China*
[2] *Institute of Microelectronics of Chinese Academy of Sciences, Beijing* 100029, *China*
[3] *Department of Microelectronics, University of Chinese Academy of Sciences, Beijing* 100049, *China*

(Received 10 May 2021; revised manuscript received 22 June 2021; accepted manuscript online 24 June 2021)

A novel 4H-SiC merged P–I–N Schottky (MPS) with floating back-to-back diode (FBD), named FBD-MPS, is proposed and investigated by the Sentaurus technology computer-aided design (TCAD) and analytical model. The FBD features a trench oxide and floating P-shield, which is inserted between the P+/N− (PN) junction and Schottky junction to eliminate the shorted anode effect. The FBD is formed by the N-drift/P-shield/N-drift and it separates the PN and Schottky active region independently. The FBD reduces not only the $V_{\rm turn}$ to suppress the snapback effect but also the $V_{\rm on}$ at bipolar operation. The results show that the snapback can be completely eliminated, and the maximum electric field ($E_{\rm max}$) is shifted from the Schottky junction to the FBD in the breakdown state.

Keywords: 4H-SiC, merged P–I–N Schottky (MPS), snapback effect, turnover voltage, floating back-to-back diode (FBD)

PACS: 85.30.–z, 73.40.Kp, 85.30.De, 72.20.Ht **DOI:** 10.1088/1674-1056/ac0e23

1. Introduction

The 4H-SiC power devices have great potential applications for their unique characteristics of high-voltage, high-frequency, and high-temperature.[1–3] The 4H-SiC Schottky barrier diode (SBD) is widely used in high-frequency area due to its unipolar conduction mode. However, the large leakage current limits its breakdown performance and high-voltage application.[4–6] The 4H-SiC P–I–N diode is widely used in high power case due to its bipolar conduction mode.[7–9] However, the poor reverse recovery limits its application in high-frequency area. The 4H-SiC merged P–I–N Schottky (MPS) diode is a promising device by integrating the Schottky and PN junction into one chip, which realizes the superior breakdown performance and fast reverse recover characteristics.[10–14] However, an undesirable snapback effect is induced by the short effect of the Schottky junction at the forward conduction, which can prevent the device from implementing full turn-on, thereby leading to unreliability for the power systems. Many advanced structures have been proposed to solve the snapback in recent years. The L-MPS can suppress the snapback by extending the length of the PN junction, and the anode resistance is increased.[15] The S-MPS can alleviate the snapback turnover voltage $V_{\rm turn}$, and the width of the PN junction is 1.5 times longer than the thickness of the N-drift.[16] The SP-MPS can not only eliminate the snapback but also reduce the leakage current, and the reverse blocking voltage is increased by the introduced shallow P region.[17] In this paper, a novel MPS with floating back-to-back diode (FBD-MPS) is proposed to eliminate the snapback and reduce the unipolar specific on-resistance $R_{\rm on}$.

2. Devices structure and equivalent circuit

The cross section schematic and equivalent circuit of conventional MPS (CON-MPS) and the FBD-MPS are shown in Fig. 1. For the CON-MPS, it has PN and Schottky junction at

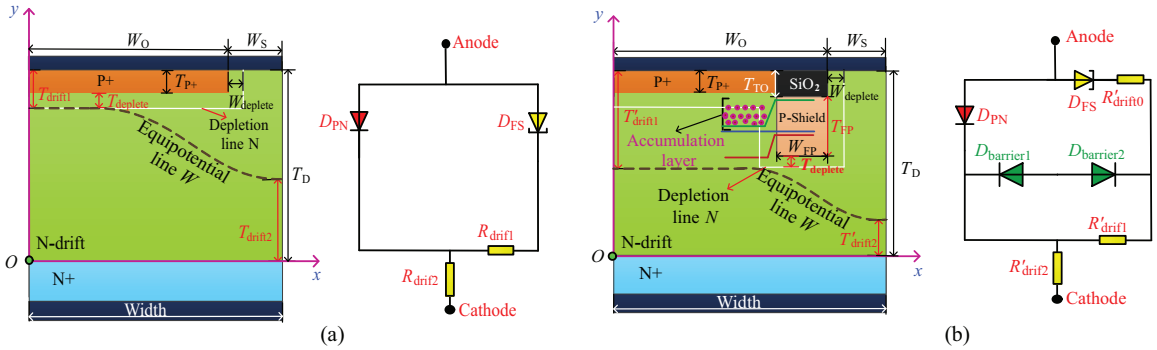


Fig. 1. (a) CON-MPS structure and equivalent circuit, and (b) proposed FBD-MPS structure and equivalent circuit, two floating backtoback diodes and $R'_{\rm drift0}$ introduced.

†Corresponding author. E-mail: 1531815309@qq.com

© 2022 Chinese Physical Society and IOP Publishing Ltd

Table 1. Device parameters of FBD-MPS and CON-MPS.

Symbol	Description	CON-MPS	FBD-MPS
$W_{\rm D}$	N-drift width (μm)	17	17
$W_{\rm O}$	PN junction (μm)	15	15
$W_{\rm FP}$	Floating P-shield width (μm)	–	1
$W_{\rm S}$	Schottky junction width (μm)	2	2
$T_{\rm D}$	N-drift thickness (μm)	35	35
$T_{\rm P+}$	P+ anode thickness (μm)	0.5	0.5
$T_{\rm TO}$	Trench oxide thickness (μm)	–	0.5
$T_{\rm FP}$	Floating P-shield thickness (μm)	–	4.5
$N_{\rm D}$	N-drift region doping ($\rm cm^{-3}$)	1×10^{15}	1×10^{15}
$N_{\rm A}$	P+ region doping ($\rm cm^{-3}$)	5×10^{18}	5×10^{18}
$N_{\rm FP}$	Floating P-shield doping ($\rm cm^{-3}$)	–	2×10^{16}

the anode electrode, thus the PIN diode $D_{\rm PN}$ and Schottky diode $D_{\rm FS}$ are formed.[18] The N-drift is divided by the equipotential line W, and the $R_{\rm drift1}$ and $R_{\rm drift2}$ are distributed in the equivalent circuit as shown in Fig. 1(a). For the FBD-MPS, a transistor N-drift/P-shield/N-drift is designed between the PN and equivalent circuit as shown in Fig. 1(b). Additionally, the FBD helps to deplete the N-drift under the Schottky junction, and an extra resistance $R'_{\rm drift0}$ is also introduced.

The key parameters of the proposed FBD-MPS and CON-MPS are compared and listed in the Table 1. The width $W_{\rm D}$ and thickness $T_{\rm D}$ of the N-drift for each of the two devices are 17.0 μm and 35.0 μm, respectively. The doping $N_{\rm D}$ of the N-drift and the $N_{\rm A}$ of the P+ anode are 1×10^{15} $\rm cm^{-3}$ and 5×10^{18} $\rm cm^{-3}$, respectively. For the FBD-MPS, the width $W_{\rm FP}$, the thickness $T_{\rm FP}$, and the doping $N_{\rm FP}$ of the P-shield are 1.0 μm, 4.5 μm, and 2×10^{16} $\rm cm^{-3}$, respectively.

3. Snapback $V_{\rm turn}$ analytical model

The N-drift for each of the CON-MPS and FBD-MPS is divided into N-drift1 and N-drift2 along the equipotential line W as indicated in Fig. 1. The $T_{\rm drift1}$ for the CON-MPS and $T'_{\rm drift1}$ for the FBD-MPS can be expressed by Eqs. (1) and (2), respectively ($T_{\rm P+}$ and $T_{\rm deplete}$ are the P+ anode thickness and the PN junction depletion thickness, respectively. $T_{\rm TO}$ is the trench oxide thickness, and $T_{\rm FB}$ is the floating P-shield thickness for the FBD-MPS). It is noted that the $T'_{\rm drift1}$ is bigger than $T_{\rm drift1}$.

$$T_{\rm drift1} = T_{\rm P+} + T_{\rm deplete}, \tag{1}$$

$$T'_{\rm drift} = T_{\rm TO} + T_{\rm deplete} + T_{\rm FB}. \tag{2}$$

The $T_{\rm drift2}$ for the CON-MPS and $T'_{\rm drift2}$ for the FBD-MPS can be expressed by Eqs. (3) and (4) (W_1 equals 0.5 μm on the assumption that the equipotential line W in lateral direction is flat within the range of $x > (W_{\rm O}+W_1)$). It is noted that the $T'_{\rm drift2}$ is lower than $T_{\rm drift2}$ because the equipotential line W is moved downward by the depletion of the P-shield.

$$\begin{aligned} T_{\rm drift2} &= \int_0^{T_{\rm D}-T_{\rm drift1}} \frac{(T_{\rm D}-y)^2}{(T_{\rm D}-y)^2+(W_{\rm O}+W_1)^2}\,{\rm d}y \\ &= T_{\rm D}-T_{\rm drift1}-(W_{\rm O}+W_1) \\ &\quad\times\left[\arctan\left(\frac{T_{\rm D}}{W_{\rm O}+W_1}\right)-\arctan\left(\frac{T_{\rm drift1}}{W_{\rm O}+W_1}\right)\right], \end{aligned} \tag{3}$$

$$\begin{aligned} T'_{\rm drift2} &= \int_0^{T_{\rm D}-T'_{\rm drift1}} \frac{(T_{\rm D}-y)^2}{(T_{\rm D}-y)^2+(W_{\rm O}+W_1)^2}\,{\rm d}y \\ &= T_{\rm D}-T'_{\rm drift1}-(W_{\rm O}+W_1) \\ &\quad\times\left[\arctan\left(\frac{T_{\rm D}}{W_{\rm O}+W_1}\right)-\arctan\left(\frac{T'_{\rm drift1}}{W_{\rm O}+W_1}\right)\right]. \end{aligned} \tag{4}$$

The specific on-resistance $R_{\rm on}$ of the CON-MPS is the sum of the $R_{\rm drift1}$ and $R_{\rm drift2}$, and the $R'_{\rm on}$ of the FBD-MPS is the sum of the $R'_{\rm drift0}$, $R'_{\rm drift1}$ and $R'_{\rm drift2}$. The effective thickness of the N-drift $T_{\rm sum}$ for the CON-MPS and $T'_{\rm sum}$ for the FBD-MPS can be expressed by Eqs. (5) and (6), because the current density through the Schottky contact is $(W_{\rm O}+W_{\rm S})/(W_{\rm S}-W_{\rm deplete})$ times the current density through the cathode contact as a result of current continuity. It is noted that the $T_{\rm sum}$ is bigger than $T'_{\rm sum}$. The $W_{\rm deplete}$ is the PN junction depletion width, which can be expressed by Eq. (7)[19]

$$T_{\rm sum} = T_{\rm D} + \left(\frac{W_{\rm O}+W_{\rm S}}{W_{\rm S}-W_{\rm deplete}}-1\right)\times T_{\rm drift1}, \tag{5}$$

$$T'_{\rm sum} = T_{\rm D} + \left(\frac{W_{\rm O}+W_{\rm S}}{W_{\rm S}-W_{\rm deplete}}-1\right)\times T'_{\rm drift1}, \tag{6}$$

$$W_{\rm deplete} = \sqrt{\frac{2\varepsilon_{\rm s}(V_{\rm PN}-V_{\rm f})}{qN_{\rm D}}}. \tag{7}$$

The voltage drop across Schottky junction $V_{\rm FS}$ for the CON-MPS and $V'_{\rm FS}$ for the FBD-MPS can be expressed by Eqs. (8) and (9) ($J_{\rm FC}$ is the cell current density, and $\phi_{\rm B}$ is the Schottky barrier height).

$$V_{\rm FS} = \phi_{\rm B} + \frac{kT}{q}\times\ln\left(\frac{J_{\rm FC}}{AT^2}\times\frac{W_{\rm O}+W_{\rm S}}{W_{\rm S}-W_{\rm deplete}}\right), \tag{8}$$

$$V'_{\rm FS} = \phi_{\rm B} + \frac{kT}{q}\times\ln\left(\frac{J_{\rm FC}}{AT^2}\times\frac{W_{\rm O}+W_{\rm S}}{W_{\rm S}-W_{\rm deplete}}\right). \tag{9}$$

The voltage drop across $R_{\rm drift2}$ equals $(V_{\rm turn}-V_{\rm FS})\times T_{\rm drift2}/T_{\rm sum}$, thus the snapback $V_{\rm turn}$ for the CON-MPS and $V'_{\rm turn}$ for the FBD-MPS can be expressed by Eqs. (10) and (11), ($V_{\rm PN}$ is built-in potential of the PN junction). It is noted that $V'_{\rm turn}$ is lower than $V_{\rm turn}$.

$$\begin{aligned} V_{\rm turn} &= V_{\rm FS} + (V_{\rm PN}-V_{\rm FS})\times\frac{T_{\rm sum}}{T_{\rm sum}-T_{\rm drift2}} \\ &= V_{\rm FS} + (V_{\rm PN}-V_{\rm FS})\times\frac{1}{1-T_{\rm drift2}/T_{\rm sum}}, \end{aligned} \tag{10}$$

$$\begin{aligned} V'_{\rm turn} &= V'_{\rm FS} + (V_{\rm PN}-V'_{\rm FS})\times\frac{T'_{\rm sum}}{T'_{\rm sum}-T'_{\rm drift2}} \\ &= V'_{\rm FS} + (V_{\rm PN}-V'_{\rm FS})\times\frac{1}{1-T'_{\rm drift2}/T'_{\rm sum}}. \end{aligned} \tag{11}$$

4. Results and discussion

Figure 2 shows the electron and potential distribution in lateral direction along $y = 34.2$ μm for the CON-MPS and FBD-MPS. The trench oxide and floating P-shield is introduced between the PN junction and the Schottky junction, thus the electrons will accumulate under the P+ anode due to the potential barrier of the P-shield as illustrated in Fig. 1(b). Therefore, the electron concentration distribution at $y = 34.2$ μm is extracted to illustrate the accumulation effect, and the potential is explored to reveal the barrier effect. In Fig. 2(a), the electron density of the FBD-MPS is two orders of magnitude higher than that of the CON-MPS at the same $V_A = 1.5$ V and 2.5 V of the unipolar mode, and it is almost the same when the devices operate in the bipolar mode at the $V_A = 3.1$ V. The variations of FBD-caused potential barrier with width at $V_A = 1.5$ V and 2.5 V of the FBD-MPS are shown in Fig. 2(b).

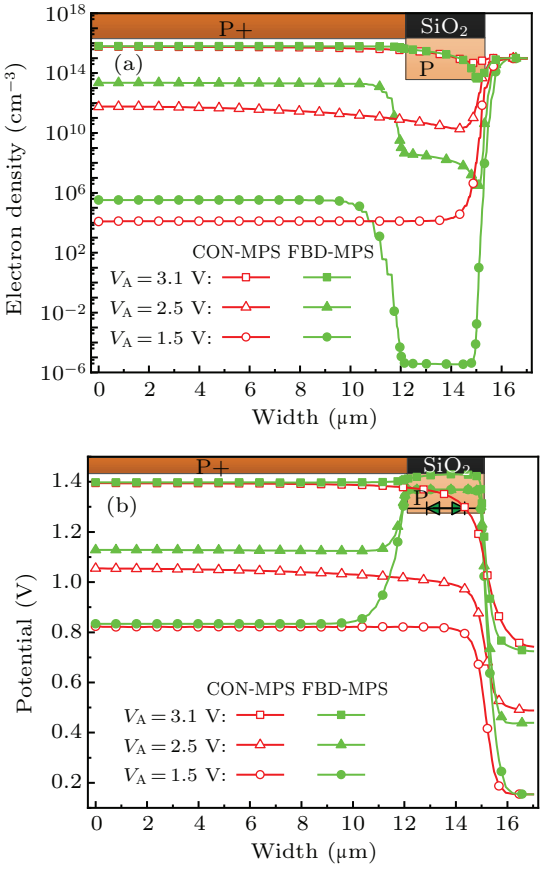


Fig. 2. Influences of width on (a) electronic density and (b) potential distribution for the devices at $y = 34.2$ μm ($W_O : W_S = 15 : 2$).

Figure 3 shows the forward *I*–*V* characteristics of the CON-MPS and proposed FBD-MPS. The snapback is observed for the device due to the short effect of the Schottky anode. The turnover voltage V_{turn} and the extent of snapback ΔV_{SB} increase with *t* Schottky junction W_S increasing. More importantly, the unipolar specific on-resistance R_{on} of the FBD-MPS is much higher than that of the CON-MPS, which is because the FBD can deplete the N-drift under the Schottky junction, and the extra resistance R'_{drift0} is introduced into the equivalent circuit.

Figure 4 demonstrates the influence of the W_S and W_O on the V_{turn}. The T_{sum} decreases with W_S increasing according to Eq. (5). Therefore, the V_{turn} increases with W_S increasing according to Eq. (10). The T_{drift2} decreases with W_O increasing according to Eq. (3), and the T_{sum} and V_{FS} increase with W_O increasing according to Eqs. (5) and (8). Therefore, the V_{turn} decreases with W_O increasing according to Eq. (10). The simulations and analytical model results are illustrated and compared together as shown in Figs. 4(a) and 4(b). The V'_{turn} of the proposed FBD-MPS is much lower than that of the CON-MPS, which is because the T'_{sum} and T'_{drift2} increase by the FBD.

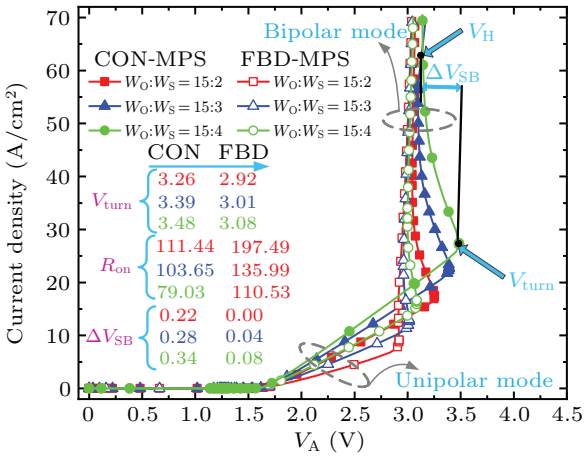


Fig. 3. Forward *I*–*V* characteristics of CON-MPS and FBD-MPS, with V_{turn} denoting turnover voltage, $\Delta V_{SB} = V_{turn} - V_H$, and R_{on} representing specific-on resistance).

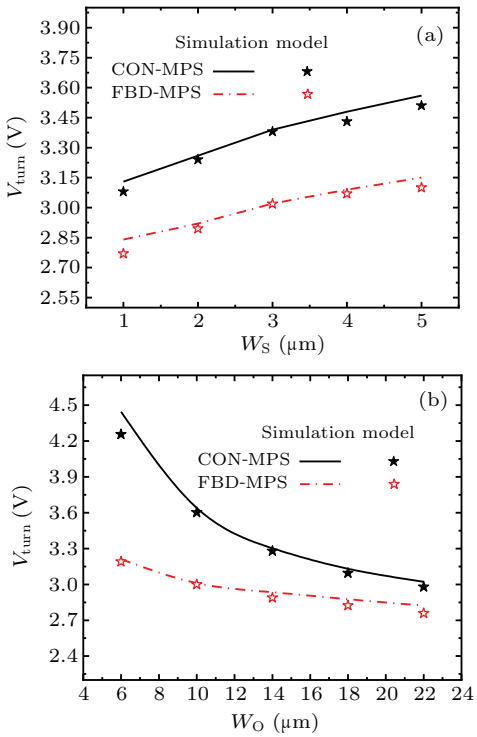


Fig. 4. Variations of V_{turn} with (a) width W_S and (b) width W_O of Schottky junction and PN junction, with closed symbols denoting results from analytical model and solid line representing simulation results.

Figure 5 demonstrates the influence of T_D and N_D on V_{turn}, ΔV_{SB}, V_{on}, and BV. For V_{turn}, T_{drift2}, and T_{sum} increase with T_D increasing according to Eqs. (3) and (5), thus V_{turn} increases with T_D increasing according to Eq. (10). Additionally, V_{turn} gradually increases with N_D increasing according to Eqs. (7) and (10) due to the increase of $W_{deplete}$. The simulations and results from the analytical model are illustrated and compared together as shown in Figs. 5(a) and 5(b). For ΔV_{SB}, the snapback is completely suppressed for the FBD-MPS when T_D is shorter than 42.0 μm as indicated in Fig. 5(a). The snapback is also completely eliminated when N_D changes from 5×10^{14} cm^{-3} to 3×10^{15} cm^{-3} as indicated in Fig. 5(b). Additionally, V_{on} increases with T_D increasing as shown in Fig. 5(a), and BV decreases with N_D increasing as shown in Fig. 5(b) for the devices.

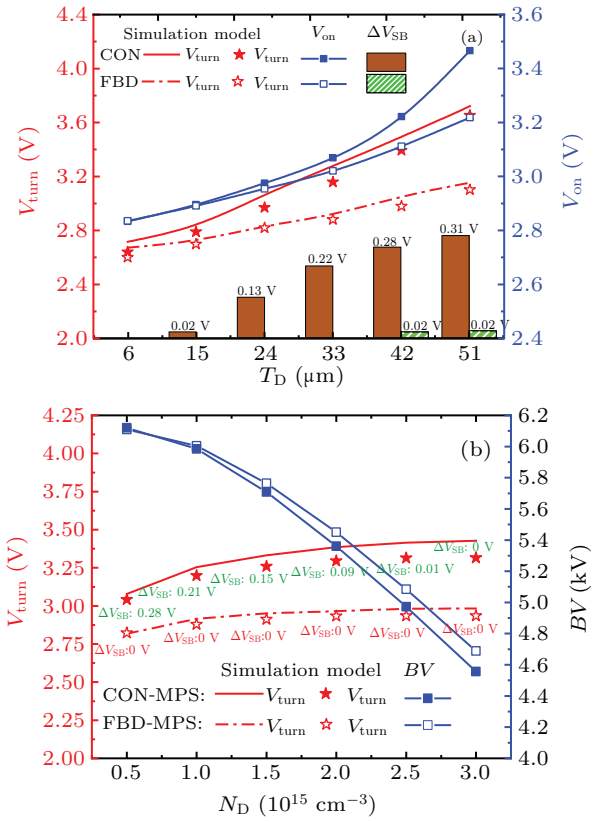


Fig. 5. (a) Variations of V_{turn} and V_{on} with thickness T_D in N-drift region for CON and FBD and (b) variations of V_{turn} and BV with doping concentration N_D. (V_{on} is the forward voltage at the current density of 100 A/cm^2, and BV is breakdown voltage at leakage current of 10^{-4} A/cm^2).

Figure 6 demonstrates the variations of V'_{turn} and BV with T_{FB} (see Fig. 6(a)) and with N_{FB} (see Fig. 6(b)) for the proposed FBD-MPS. For V'_{turn}, T'_{drift1} increases and T'_{drift2} decreases with T_{FB} increasing according to Eqs. (2) and (4), respectively. Thus V'_{turn} increases with the augment of T_{FB} according to Eq. (11). The simulations and results from the analytical model are illustrated and compared together as shown in Fig. 6(a). The V'_{turn} is almost the same when N_{FB} increases from 5.0×10^{15} cm^{-3} to 3.0×10^{16} cm^{-3} in Fig. 6(b), which is because the $W_{deplete}$ and T'_{sum} do not depend on the N_{FB} according to Eqs. (7) and (6). For ΔV_{SB}, the snapback can be completely suppressed when T_{FB} is higher than 4.0 μm in Fig. 6(a), and the snapback is also completely eliminated when N_{FB} changes from 5×10^{15} cm^{-3} to 3×10^{16} cm^{-3} in Fig. 6(b). The value of BV reaches the maximum at $T_{FB} = 4.0$ μm in Fig. 6(a) and at $N_{FB} = 1.5\times10^{16}$ cm^{-3} in Fig. 6(b).

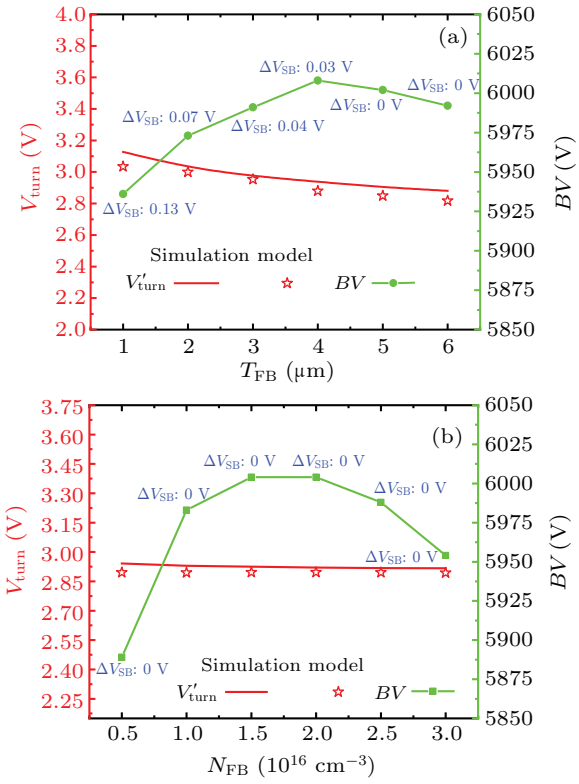


Fig. 6. Variations of V'_{turn} and BV with (a) T_{FB} and (b) N_{FB} of FBD ($W_O : W_S = 15 : 2$).

Figure 7 shows the lateral electric field distributions at $y = 34.5$ μm for the devices. The maximum electric field E_{max} for the FBD-MPS is shifted from the Schottky junction to the FBD. However, the avalanche breakdown BV for the CON-MPS and FBD-MPS are both 6000 V as shown in the inset.

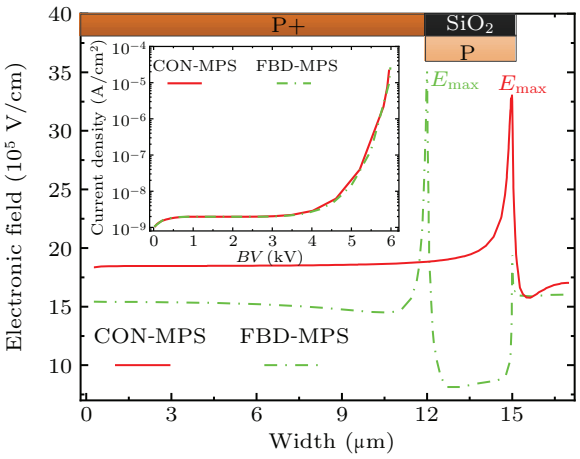


Fig. 7. Curves of E_{max} and BV *versus* width for FBD-MPS and conventional CON-MPS at $y = 34.5$ μm ($W_O : W_S = 15 : 2$).

Figure 8 displays the reverse recovery characteristics of the devices. The reverse recovery time t_{rr} is 2.7×10^{-8} s for

the CON-MPS and FBD-MPS. The Q_{rr} of FBD-MPS is bigger than that of the CON-MPS because more holes are injected at the forward conduction, and it decreases with theenhancement of W_S for each of the two devices. The values of softness factor S are bigger than 1 and gradually increase with the rise of the W_S, thus the soft reverse recovery is guaranteed.

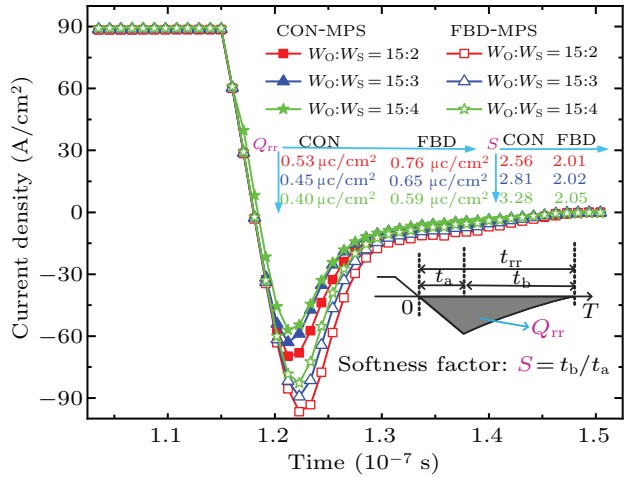


Fig. 8. Recovery waveforms of devices, with Q_{rr} denoting shadow area, t_{rr} representing reverse recovery time, and $S = t_b/t_a$.

5. Conclusions

In this work, a novel 4H-SiC MPS with floating back-to-back diode (FBD) is proposed and investigated by using the simulation and analytical models. The V_{turn} analytical models of the snapback are established and well matched with the simulation results, and V_{turn} can decrease by reducing the ratio W_S/W_O, T_D and N_D for the CON-MPS and FBD-MPS. More importantly, the V_{turn} can be effectively reduced by enhancing the T_{FB} for the FBD-MPS.

References

[1] Zhao F and Islam M M 2010 *IEEE Electron Dev. Lett.* **31** 1146
[2] Shen P, Wang Y, Li X J, Yang J O, Yu C H and Cao F 2021 *Chin. Phys. B* **30** 058502
[3] Singh R, Cooper J A, Melloch M R, Chow T P and Palmour J W 2002 *IEEE Trans. Electron. Dev.* **49** 665
[4] Baliga B J 1984 *IEEE Electron Dev. Lett.* **5** 194
[5] Zhao J H, Alexandrov P and Li X 2003 *IEEE Electron Dev. Lett.* **24** 402
[6] Lee K, Wang S and Chan L 2017 *IEEE Trans. Electron. Dev.* **64** 1394
[7] Hiyoshi T, Hori T, Suda J and Kimoto T 2008 *IEEE Trans. Electron Dev.* **55** 1841
[8] Wang C, L Su and Zhang L 2018 *1st Workshop on Wide Bandgap Power Devices and Applications in Asia*, May 16–18, 2019, Xi'an, China, p. 221
[9] Fedison J B, Ramungul N, Chow T P, Ghezzo M and Kretchmer J W 2001 *IEEE Electron Dev. Lett.* **22** 130
[10] Wu J, Ren N and Sheng K 2019 *Proceedings of the 31st International Symposium on Power Semiconductor Devices*, May 19–23, 2019, Shanghai, China, p. 203
[11] Du Q and Tao X 2020 *IEEE Trans. Electron Dev.* **67** 4033
[12] Huang J H, Lv H L, Li X J, Zhang Y M, Zhang Y M, Tang X Y, Chen F P and Song Q W 2011 *Chin. Phys. B* **20** 118401
[13] Huang Y and Wachutka G 2016 *International Conference on Simulation of Semiconductor Processes and Devices*, September 6–8, 2016, Nuremberg, Germany, p. 117
[14] d'Alessandro V, Irace A, Breglio G, Spirito P, Bricconi A, Carta R, Raffo D and Merlin L 2006 *18th International Symposium on Power Semiconductor Devices and ICs*, June 4–8, 2006, Naples, Italy, p. 1
[15] Sawant S and Baliga B J 1998 *10th International Symposium on Power Semiconductor Devices and ICs*, June 3–6, 1998, Kyoto, Japan, p. 297
[16] Niwa H, Suda J and Kimoto T 2017 *IEEE Trans. Electron Dev.* **64** 874
[17] Park J, Park K S, Won J I, Kim K H, Koo S, Kim S G and Mun J K 2017 *Appl. Phys. Lett.* **110** 142103
[18] Huang Y, Erlbacher T, Buettner J and Wachutka G 2016 *28th International Symposium on Power Semiconductor Devices and ICs*, June 12–16, 2016, Prague, Czech Republic, p. 63
[19] Zhu L and Chow T P 2008 *IEEE Trans. Electron Dev.* **55** 1857